# VIII. APPLIED PLASMA RESEARCH*

## A. Active Plasma Systems

### Academic Research Staff

Prof. L. D. Smullin
Prof. R. J. Briggs
Prof. R. R. Parker
Prof. K. I. Thomassen

### Graduate Students

S. P. Hirshman
J. L. Kulp, Jr.
J. A. Mangano
M. I. Mirkin
G. H. Neilson
M. Simonutti
A. E. Throop
P. R. Widing

### 1. EFFECT OF OBLIQUENESS BETWEEN DENSITY GRADIENT AND MAGNETIC FIELD ON RESONANCE CONES NEAR THE LOWER HYBRID RESONANCE

A recent publication[1] deals extensively with the phenomena of "resonance cones" in homogeneous plasma. This term describes the surface on which the spatial response of a localized RF excitation is confined in a plasma. In a previous report,[2] we have examined this effect near lower hybrid resonance for a plasma with a density gradient transverse to the magnetic field.

Most analyses of plasma waves near lower hybrid resonance in the presence of a density gradient deal with a model in which that gradient is exactly perpendicular to the uniform magnetic field. Fluctuations, however, in a plasma or the transport of plasma away from a localized plasma generation region would be associated with a finite component of density gradient in the direction of the magnetic field. This report points out that this slight obliqueness between the density gradient and magnetic field can cause significant changes in the resonance cones near lower hybrid resonance.

Our specific study concerns spatially localized RF wave propagation in a plasma from a region of low density through a region of increasing density toward a layer associated with lower hybrid resonance. It is assumed that $m_e/m_i \ll \omega_{pe}^2/\omega_{ce}^2 \ll 1$, which implies that $\omega_{LH} \approx \omega_{pi}$. In our previous analysis of the case of perpendicular density gradient and magnetic field,[2] a one-dimensional density inhomogeneity of linear profile was considered. This geometry is illustrated in Fig. VIII-1. The resulting two-dimensional resonance-cone signal paths produced by localized RF excitation at the low-density edge of the plasma are shown in Fig. VIII-2. The paths are two symmetric parabolic segments emanating from the source region and reaching tangentially the density layer corresponding to lower hybrid resonance. The wave energy is absorbed there according to cold-plasma theory.

---

*This work was supported by the National Science Foundation (Grant GK-28282X).

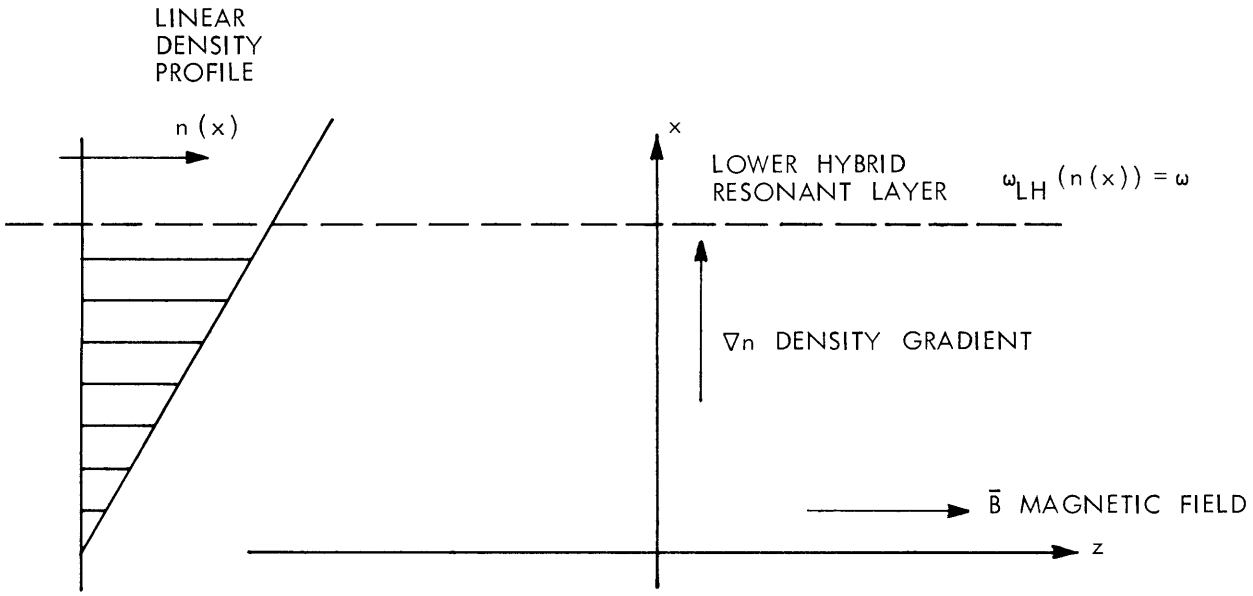


Fig. VIII-1. Geometry of the problem for $\nabla n \perp \bar{B}$.

The signal paths are determined by following through the plasma the direction parallel to the group velocity of an electrostatic plane wave. These paths can be expressed by

$$\frac{dx}{dz} = \pm \sqrt{\frac{-K_{\perp}(x)}{K_{\parallel}(x)}}, \tag{1}$$

where $K_{\perp}$ and $K_{\parallel}$ are components of the cold-plasma dielectric tensor. Note that since

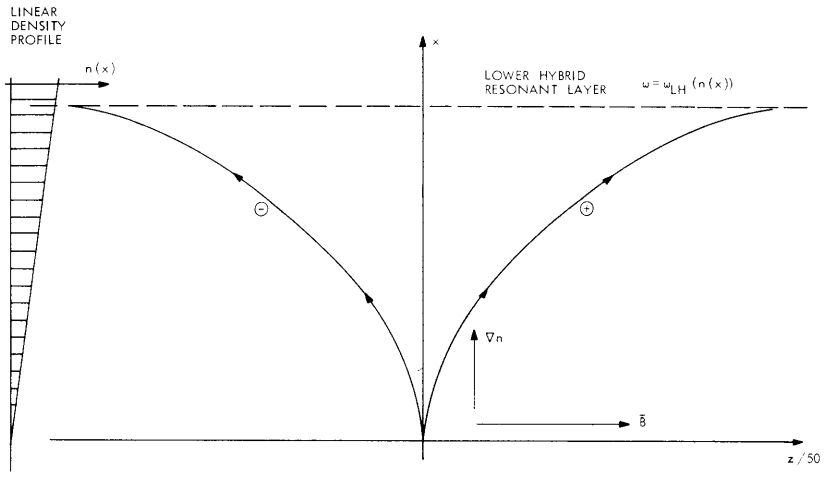


Fig. VIII-2. Signal paths for $\nabla n \perp \bar{B}$.

the layer of lower hybrid resonance is determined by the relation $K_\perp(x) = 0$, the signal path becomes tangent to the z direction at lower hybrid resonance.

When the model is generalized to allow for an arbitrary angle between the density gradient and uniform magnetic field, it can be shown that the lower hybrid resonance layer is no longer the only characteristic density layer of the problem. The generalized geometry of the model is illustrated in Fig. VIII-3, where $\alpha$ is defined as the angle between the density gradient and the perpendicular to the magnetic field, and a new set of the coordinate axes x', z' is defined. The z direction is still the direction of homogeneity, while the z' direction is parallel to the magnetic field. The signal-path formula can be written directly in terms of the primed coordinate system, since the magnetic field is now in the z' direction.

$$\frac{dx'}{dz'} = \pm \sqrt{\frac{-K_\perp(x', z')}{K_{||}(x', z')}}. \tag{2}$$

In terms of the unprimed coordinate system, $K_\perp$ and $K_{||}$ are functions only of x. Equation 2 can be transformed to the unprimed coordinate system, with the result that

$$\frac{dx}{dz} = \frac{\sqrt{\frac{-K_\perp(x)}{K_{||}(x)}} + \tan\alpha}{1 - \sqrt{\frac{-K_\perp(x)}{K_{||}(x)}}\tan\alpha}, \tag{3}$$

which corresponds to taking the plus sign in Eq. 2, and

$$\frac{dx}{dz} = \frac{-\sqrt{\frac{-K_\perp(x)}{K_{||}(x)}} + \tan\alpha}{1 + \sqrt{\frac{-K_\perp(x)}{K_{||}(x)}}\tan\alpha}, \tag{4}$$

which corresponds to taking the minus sign.

Again, the result is two signal paths emanating from the source region, although the paths are no longer symmetric. The signal paths determined by Eqs. 3 and 4 are plotted in Fig. VIII-4 for the case of linear density profile, and for $\alpha = \tan^{-1}\sqrt{m_e/m_i} \approx \sqrt{m_e/m_i}$. This $\alpha$ is generally a small number corresponding to 1.3° for a hydrogen plasma, even less for a plasma of heavier ions. Note that compression of the z' coordinate by a factor of 50 gives the appearance of a much larger $\alpha$ in

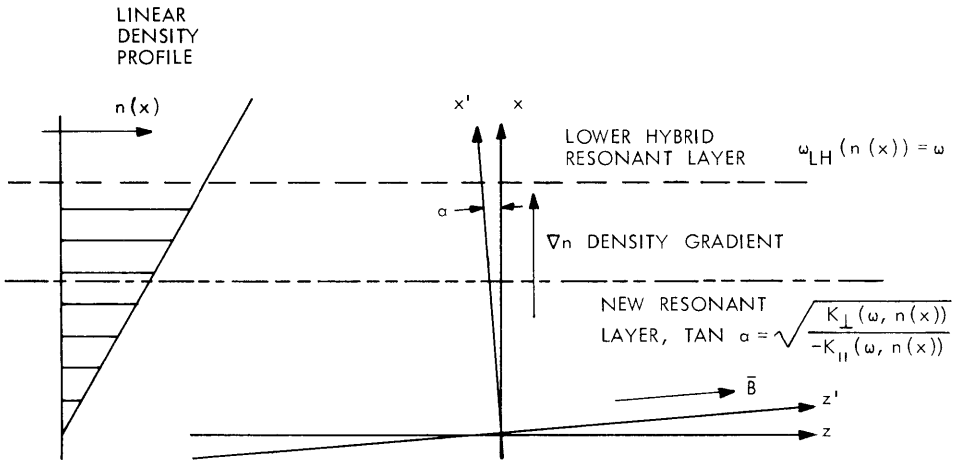


Fig. VIII-3. Geometry allowing obliqueness between ∇n and $\bar{B}$.

Fig. VIII-4. The new signal paths have significant differences from those of the less general case. Path 3, corresponding to Eq. 3, reaches hybrid resonance, but, as can be shown by more complete analysis of the problem, it reflects at the lower hybrid resonance layer into the mode determined by Eq. 4 (path 4a). The path then becomes asymptotic to a particular density layer of density one half of that at lower hybrid

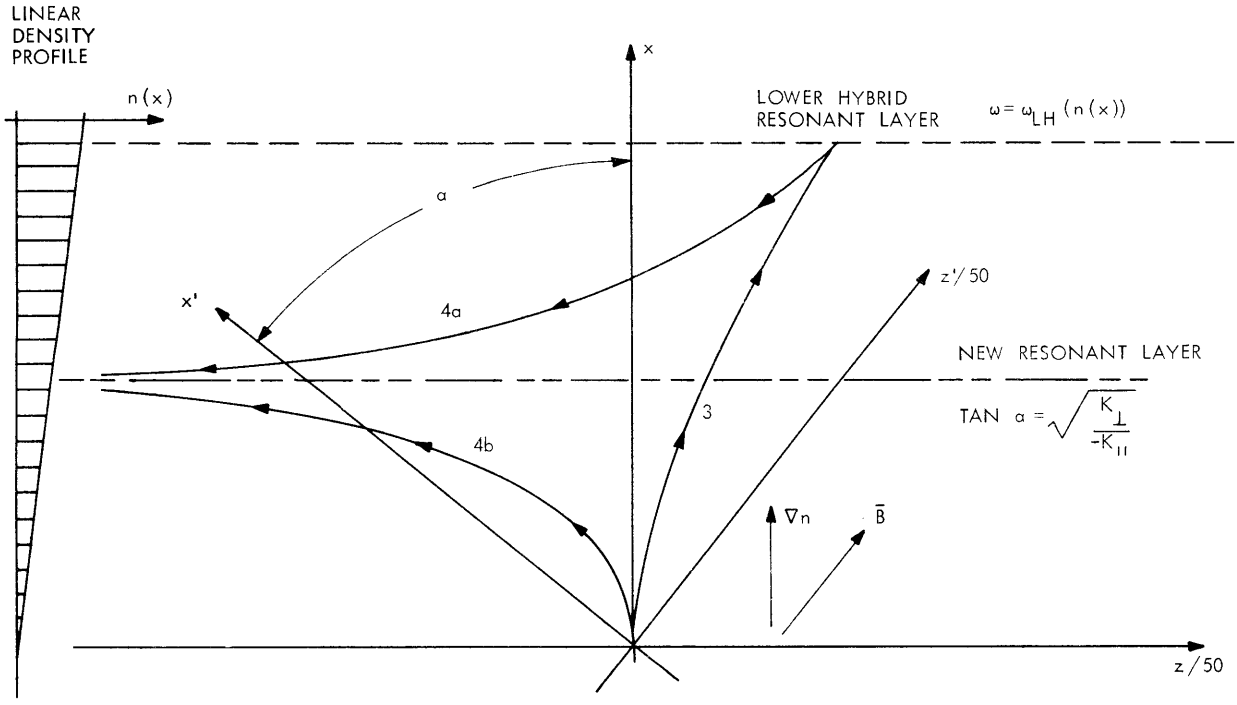


Fig. VIII-4. Signal paths for the case of oblique ∇n and $\bar{B}$.

resonance for the condition $\alpha = \sqrt{m_e/m_i}$. The other branch (path 4b) becomes directly asymptotic to this new density layer. This new density layer is determined in general by the condition $\tan \alpha = \sqrt{-K_\perp/K_\parallel}$ under which the right-hand side of Eq. 4 is zero.

It is important to point out that for any nonzero $\alpha$, the signal power is not absorbed at the new density layer. Instead, analysis by cold-plasma theory shows that the power is now directed to infinity in the -z direction. Therefore, setting $\alpha$ exactly equal to zero changes the physical picture significantly in certain respects. This suggests that a finite $\alpha$ should be included in the analysis of lower hybrid resonance in an inhomogeneous plasma.

The reason for this marked difference may be explained as follows. The numerator of Eq. 4 goes to zero at some density layer determined by $\tan \alpha = \sqrt{-K_\perp(x)/K_\parallel(x)}$. When the right-hand side of (4) is linearized about this value of x, the resulting differential equation has a logarithmic singularity at that value of x, which is the new resonant density layer. When $\alpha$ is exactly zero, however, linearization of the right-hand side of (4) is not possible and the singularity, which was a result of the linear term, does not appear.

M. Simonutti, R. R. Parker, R. J. Briggs

References

1. R. K. Fisher and R. W. Gould, Phys. Fluids 14, 857 (1971).
2. R. R. Parker, Quarterly Progress Report No. 102, Research Laboratory of Electronics, M.I.T., July 15, 1971, pp. 97-111.

## 2. IMPEDANCE OF ELECTROSTATIC COUPLERS IN AN INHOMOGENEOUS PLASMA

In this report we outline a theoretical calculation of the impedance of the electrostatic couplers used in our lower hybrid wave experiments.[1] In this coupling method, the RF voltage is applied to a narrow metal ring separated from a grounded metal cylinder by two narrow gaps. The slab geometry approximation to this structure is illustrated in Fig. VIII-5.

We assume that the plasma density next to the structure is such that $K_\parallel(0) < 0$, so that the solution for the RF potential near the structure can be written[2]

$$\phi(x, z) = A(x) \int_{-\infty}^{+\infty} \phi_o(k_z) \exp\left[-ik_z z + i\int_0^x k_x\, dx\right] \frac{dk_z}{2\pi}, \tag{1}$$

where

$$A(x) = \left[K_{\parallel}(0)\, K_{\perp}(0)/K_{\parallel}(x)\, K_{\perp}(x)\right]^{1/4}$$

$$k_x = |k_z|\left[-K_{\parallel}/K_{\perp}\right]^{1/2}, \tag{2}$$

and $\phi_o(k_z)$ is the Fourier spectrum of the boundary potential, with $\phi(x = 0, z)$. If the inner ring is sufficiently thin, the net charge on the inner surface of the ring ($x = 0^+$) can be calculated as

$$q = \ell \int_{-z_1}^{z_1} \epsilon_o K_{\perp}(0)\, E_x(0, z)\, dz, \tag{3}$$

where $\ell$ is the length of the ring ($2\pi R$, with R the ring radius). With the wall potential

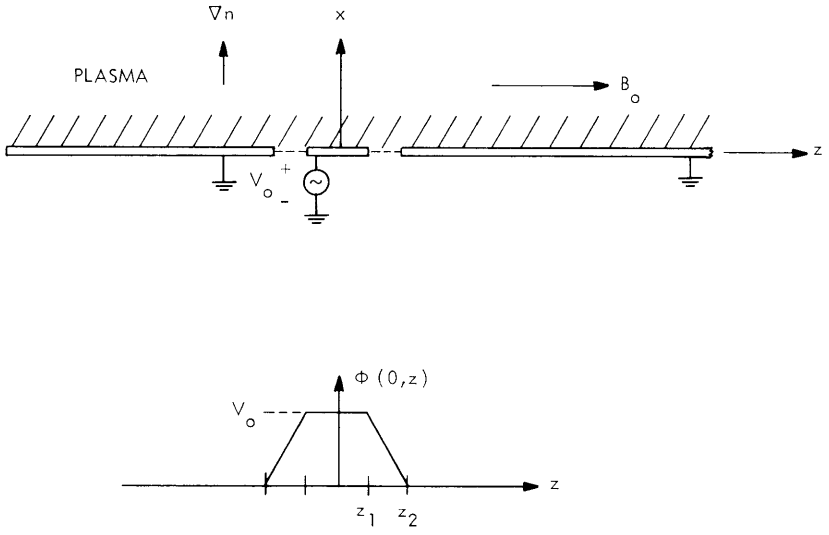


Fig. VIII-5. Electrode geometry and boundary potential.

profile of the form shown in Fig. VIII-5, we find the following expresssion for the admittance associated with the inner surface of the ring:

$$Y_1 = \frac{i\omega q}{V_o} = \frac{2}{\pi}\, \omega \epsilon_o \ell \left[-K_{\parallel}(0)\, K_{\perp}(0)\right]^{1/2} F(a), \tag{4}$$

with

$$F(a) = (1-a)^{-1}\left[\ln\left(\frac{1+a}{1-a}\right) + a \ln\left(\frac{1-a^2}{4a^2}\right)\right] \tag{5}$$

and $a = z_1/z_2$. Typical values of F are listed as follows.

| $z_1/z_2 = a$ | $F(a)$ |
|---|---|
| 0.25 | 2.48 |
| 0.50 | 1.9 |
| 0.75 | 1.6 |

Note that the total admittance of the ring structure is $Y_1$ in parallel with the capacitance associated with the outer surface of the ring ($x = 0^-$).

We see that in the regime of interest [$K_\perp(0) > 0$ and $K_\parallel(0) < 0$], $Y_1$ is purely real; physically, this comes about because all Fourier components of the electrostatic field propagate away from the structure in this regime, in contrast to the vacuum case, in which the potential is a Fourier superposition of waves that are evanescent in the x direction. In fact, this method of deriving the input admittance indicates that, in general, the (partial) input admittance of structures of this type would be purely real, with a conductance value equal to the magnitude of the capacitive admittance of the inner surface of the structure under vacuum conditions multiplied by $(-K_\parallel K_\perp)^{1/2}$.

If $\omega_p(0) = \omega_{pw} \gg \omega$, and $\omega_{pw} \ll \omega_c$, as is typically the case, then

$$Y_1 \approx \frac{2}{\pi} \omega_{pw} \epsilon_o \ell F(a)$$

is independent of frequency. With plasma densities near the structure of order $10^9$ cm$^{-3}$, the typical values of $1/Y_1$ are in the range 100-200 Ω.

R. J. Briggs

## References

1. M. Simonutti, R. R. Parker, R. J. Briggs, Quarterly Progress Report No. 104, Research Laboratory of Electronics, M.I.T., January 15, 1972, pp. 196-201.

2. R. R. Parker, Quarterly Progress Report No. 102, Research Laboratory of Electronics, M.I.T., July 15, 1971, pp. 97-111.

# VIII. APPLIED PLASMA RESEARCH*

## C. Plasma Effects in Solids


Academic Research Staff

Prof. A. Bers

Graduate Students

J. F. Cafarella


### 1. NONLINEAR PLASMA EFFECTS IN INTERACTIONS WITH ACOUSTIC WAVES

We have recently proposed to study the surface acoustoelectric current in order to determine the mobility and trapping of electrons at the surface of a semiconductor.[1] The phenomenon of acoustoelectric current is a nonlinear effect arising from the bunching of electrons by the fields of an acoustic wave.[2] In previous studies of this phenomenon[2] either the effects of electron diffusion, or electron drift, or both, had been neglected. Since we propose to make measurements as a function of frequency, diffusion effects may become important. Furthermore, acoustoelectric current measurements in the presence of drift can give an indication of electron density inhomogeneities.[3] Hence the effects of drift are also important. In this report we reexamine the nonlinear theory of the acoustoelectric current and derive this nonlinear current, correct to second order in field amplitudes, including both the effects of electron diffusion and drift. In a future report we shall describe the effects of trapping.

#### Nonlinear Conservation Theorem

It is usually convenient to relate the acoustoelectric current to the power dissipated or gained by the acoustic wave. For this we must employ a nonlinear energy conservation equation for the electrons. We model the electrons by hydrodynamic equations that are valid for frequencies $\omega$ which are low compared with their collision frequency $\nu$, and wavelengths $2\pi/k$ that are short compared with the electron's mean-free path $v_T/\nu$. For simplicity, we assume only a one-dimensional variation. The equations of current, continuity, and momentum are

$$\Gamma = nv \tag{1}$$

$$\frac{\partial n}{\partial t} + \frac{\partial \Gamma}{\partial z} = 0 \tag{2}$$


*This work was supported by the National Science Foundation (Grant GK-28282X), and in part by M. I. T. Lincoln Laboratory Purchase Order No. CC-544.

$$\nu m v + \frac{\kappa T}{n} \frac{\partial n}{\partial z} = qE. \tag{3}$$

Using the electrostatic current equation from Maxwell's equation

$$\epsilon \frac{\partial E}{\partial t} + J = -J_{ext}, \tag{4}$$

where $J_{ext}$ is due to the external fields, we can find the following conservation equation

$$\frac{\partial}{\partial t}\left[\frac{1}{2}\epsilon E^2 + n\kappa T \log \frac{n}{n_o}\right] + \frac{\partial}{\partial z}\left[\kappa T\left(1 + \log \frac{n}{n_o}\right)\Gamma\right] + \nu m v \Gamma = P_{ext}, \tag{5}$$

where $P_{ext}$ is the power supplied by the external fields. We note that in the steady state this power is taken up partly by power dissipated by the electrons and partly as power flow caused by electron diffusion, the third and second terms on the left-hand side of Eq. 5, respectively.

The power flow and power dissipated can be evaluated to second order in field amplitudes by iterating Eqs. 1-3. To first order we obtain the small-signal equations

$$\Gamma_1 = n_o v_1 + n_1 v_o \tag{6}$$

$$\frac{\partial n_1}{\partial t} + \frac{\partial \Gamma_1}{\partial z} = 0 \tag{7}$$

$$v_1 + D \frac{1}{n_o} \frac{\partial n_1}{\partial z} = -\mu E_1 \tag{8}$$

which, together with Poisson's equation, when Fourier-analyzed $[\exp j(\omega t - kz)]$, give the linear conductivity function $(J_1 = \sigma(\omega, k) E_1)$

$$\sigma(\omega, k) = \frac{\omega \sigma_o}{\omega - k v_o - j k^2 D} \equiv \sigma_r(\omega, k) + j\sigma_i(\omega, k), \tag{9}$$

where $\sigma_o$ is the dc conductivity, $v_o = -\mu E_o$ is the dc drift velocity, and $D = -\mu\kappa T/q$ is the diffusion constant. From these equations we can derive the small-signal conservation equation in the usual way[4] and find

$$\frac{\partial}{\partial t}\left[\frac{1}{2}\epsilon E_1^2 + \frac{1}{2}\frac{\kappa T}{n_o} n_1^2\right] + \frac{\partial}{\partial z}\left(\frac{\kappa T}{n_o} n_1 \Gamma_1\right) + \nu m v_1 \Gamma_1 = p_{ext\,1}. \tag{10}$$

The last two terms in Eq. 10 give us the small-signal power flow and power dissipated, respectively. In general, they are not the same as the respective power

terms from Eq. 5 evaluated to second order. From Eqs. 1-3 we can find the equations for the second-order fields.

$$\Gamma_2 = n_o v_2 + n_2 v_o + n_1 v_1 \tag{11}$$

$$\frac{\partial n_2}{\partial t} + \frac{\partial \Gamma_2}{\partial z} = 0 \tag{12}$$

$$\Gamma_2 + D \frac{\partial n_2}{\partial z} = -\mu(n_o E_2 + n_2 E_o + n_1 E_1). \tag{13}$$

Equations 11-13, together with Poisson's equation

$$\epsilon \frac{\partial E_2}{\partial z} = q n_2, \tag{14}$$

can be combined to give the second-order density $n_2$ as generated by the first-order fields

$$\frac{\partial n_2}{\partial t} + v_o \frac{\partial n_2}{\partial z} - D \frac{\partial^2 n_2}{\partial z^2} + \omega_\sigma n_2 = \mu \frac{\partial}{\partial z}(n_1 E_1), \tag{15}$$

where $\omega_\sigma = \sigma_o/\epsilon$ is the dielectric relaxation frequency. Now, consider the first-order fields as being established by weak coupling to an acoustic wave. All first-order field quantities will then have as time-space dependence the form $\exp j(\omega t - kz)$, where we take $\omega$ as real, and $k = k_r + jk_i$ with $|k_i| \ll |k_r|$. Equation 15 then shows that to zero order in $k_i$ the time-averaged second-order density $\langle n_2 \rangle$ is zero, and hence $\langle E_2 \rangle$ and $\langle v_2 \rangle$ are also zero. We can now evaluate to second order in field amplitudes the power-flow and power-dissipated terms of Eq. 5. We shall be interested only in their time averages and find

$$\langle p_2 \rangle = \langle (\nu m v \Gamma)_2 \rangle$$

$$= \nu m \langle v_1 \Gamma_1 \rangle + E_o q \langle \Gamma_2 \rangle \tag{16}$$

$$\langle s_2 \rangle = \left[ \kappa T \frac{\langle n_1 \Gamma_1 \rangle}{n_o} + \langle \Gamma_2 \rangle - \frac{\Gamma_o \langle n_1^2 \rangle}{2 n_o^2} \right]. \tag{17}$$

The first term, in both expressions, corresponds to what would be obtained from the small-signal conservation equation (Eq. 10).

Acoustoelectric Current

The acoustoelectric current is obtained from the time average of Eq. 13. Using the results that we found for the second-order fields, we have

$$J_{AE} \equiv \langle J_2 \rangle = -q\mu \langle n_1 E_1 \rangle$$

$$= -\frac{1}{2} |E_1|^2 \frac{\mu \sigma_r(\omega, k)}{v_a}. \tag{18}$$

Thus we verify the correctness of the usual result for $J_{AE}$.[3]

Consider now an acoustic surface wave interacting with an accumulation layer of

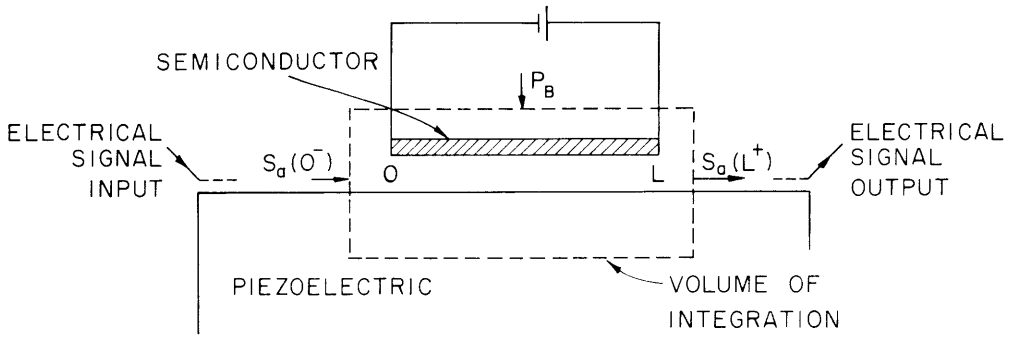


Fig. VIII-6. Configuration for surface acoustoelectric interaction.

electrons which we model as a sheet of electrons,[5] as shown in Fig. VIII-6. The surface acoustoelectric current is then simply $K_{AE} = \tau J_{AE}$, where $\tau$ is the thickness of the electron sheet. Finally we integrate, over the volume shown in Fig. VIII-6, the time average of Eq. 5 expressed to second order, and note that $\langle P_{ext} \rangle$ contains both acoustic power flow and power supplied by the dc source. The latter just cancels the second term of Eq. 16, and we obtain

$$\langle S_a(L^+) \rangle - \langle S_a(0^-) \rangle = -\tau L \frac{1}{2} |E_1|^2 \sigma_r(\omega, k), \tag{19}$$

where L is the length of the electron sheet. Using this result in Eq. 18, we find

$$K_{AE} = \frac{\mu}{L v_a} \left[ \langle S_a(L^+) \rangle - \langle S_a(0^-) \rangle \right]. \tag{20}$$

Equation 20 shows that by measuring the surface acoustoelectric current and acoustic power flow we can determine the surface mobility of the electrons.

A. Bers

References

1. J. Cafarella and A. Bers, Quarterly Progress Report No. 104, Research Laboratory of Electronics, M.I.T., January 15, 1972, pp. 217-223.

2. G. Weinriech, Phys. Rev. 104, 321 (1956); G. Weinreich and H. G. White, Phys. Rev. 106, 1104 (1957); K. A. Ingebrigtsen, J. Appl. Phys. 41, 2 (1970).

3. W. C. Wang, Phys. Rev. Letters 9, 443 (1962); J. H. McFee, in W. P. Mason (Ed.), Physical Acoustics, Vol. 4, Part A (Academic Press, Inc., New York, 1966), pp. 36-37.

4. A. Bers, Invited Proceedings of the 1970 Ultrasonics Symposium, IEEE Publication No. 70C69SU, New York, 1971, p. 169.

5. B. E. Burke, A. Bers, H. I. Smith, R. A. Cohen, and R. W. Mountain, Proc. IEEE 58, 1775 (1970).